Light-Scattering Investigation of the Temperature-Driven Conformation Change in Xanthan

Laurel S. Hacche, Gary E. Washington, and David A. Brant*

Department of Chemistry, University of California, Irvine, California 92717.
Received July 28, 1986

ABSTRACT: Low molecular weight xanthan fractions were prepared by ultrasonic degradation of high molecular weight commercial xanthan followed by extensive centrifugation and filtration, fractional precipitation, exhaustive dialysis, and conversion to the sodium salt form by ion exchange. The weight-average molecular weight, $\bar{M}_w$, root-mean-square z-average radius of gyration, $\langle s^2\rangle_z^{1/2}$, and osmotic second virial coefficient, A'_2, were measured by total intensity Rayleigh light scattering as functions of temperature, T, and added salt concentration, I, in aqueous NaCl solution; corresponding measurements of specific optical rotation, $[\alpha]_\lambda$, and intrinsic viscosity, $[\eta]$, were also carried out. At 23 and 51 °C $\bar{M}_w$ and $\langle s^2\rangle_z^{1/2}$ were found to increase by factors of 1.8 and 1.5, respectively, with I increasing from 0.004 to 0.100 M, whereas A'_2 decreased with increasing I. Under these conditions $\bar{M}_w$ and $\langle s^2\rangle_z^{1/2}$ were sensibly independent of T, but A'_2 increased with T for $I < 0.01$ M. Investigations of the details of the T dependence at $I = 0.005$ M suggest that in the temperature range between the conformational transition temperature, $T_m \simeq 45$ °C, defined by the sigmoid T dependence of $[\alpha]_\lambda$, and the highest accessible temperature, ca. 70 °C, both the molecular weight ($\bar{M}_w$) and molecular dimensions ($\langle s^2\rangle^{1/2}$ and $[\eta]$) increase above their values at lower temperatures. In these experiments A'_2 also displayed a pronounced sigmoid increase with T, but with a characteristic midpoint temperature about 10 deg greater than the chirooptically detected T_m. These data are explained qualitatively using a double-strand model for the native (ordered) xanthan, present at temperatures well below T_m, which at high enough T is expected to dissociate completely to single strands. At the highest temperatures accessible to the present light-scattering experiments the equilibrium system is postulated to contain partially dissociated double-strand dimers as well as clusters comprising more than two chains, which account for the increases in $\bar{M}_w$ and $\langle s^2\rangle_z^{1/2}$ with T. It is shown using modern polyelectrolyte theory that partial dissociation of the double-stranded dimeric clusters present at low T is expected to lead to a large increase in A'_2, with T, provided the experiments are conducted with I low enough to render dominant the Donnan contribution to A'_2.

Introduction

Xanthan is a commercially important polysaccharide produced by fermentation with the bacterium *Xanthomonas campestris*.[1,2] The polymer has a linear (cellulosic) backbone consisting of 1→4-linked β-D-glucose residues. A three-sugar substituent group is attached at C(3) of every second backbone glucose to produce a regularly repeating copolymer with comblike branching. Structural details of the five-sugar repeating unit are given elsewhere.[3,4] For present purposes it will suffice to observe that in the side chain the proximal α-D-mannose residue is normally acetylated at C(6) and that the distal β-D-mannose may bear a pyruvic acid residue in ketal linkage at C(4) and C(6). The degrees of acetyl and pyruvyl substitution, DS_{ace} and DS_{pyr}, are defined as the fractions of the respective sites substituted. In addition to the carboxyl group present on each pyruvyl-substituted side chain, every side chain carries one carboxyl group from the central β-D-glucuronic acid residue. A typical xanthan sample with $DS_{pyr} = 0.6$ thus has an average of 1.6 carboxylate charges per five-sugar repeating unit at neutral pH.

In aqueous solution xanthan undergoes a rather diffuse temperature-driven conformational transition that is most often observed by following changes in the specific optical rotation $[\alpha]_\lambda$ at fixed wavelength λ;[5-11] ^{1}H NMR measurements of the acetyl and pyruvyl methyl resonances appear to provide an alternative probe of the transition[7] as do viscosity[5,6,8] and calorimetric[9,10] measurements. The chirooptically detected transition typically spans a temperature range of 20–40 °C.[6,7,10,11] A characteristic temperature for the transition, which depends on molecular weight,[12,13] pH,[12] DS_{ace},[14] DS_{pyr},[15,16] and added salt concentration,[6,7,10,11] can be defined as the temperature at the midpoint of this temperature range. The breadth of the transition is clearly due in part to chemical and molecular weight heterogeneity of the samples in question and to the relatively small enthalpy change associated with the process.[9,10,17] Attempts to characterize the cooperativity of the transition[10,16,17] are complicated by the difficulty of separating the contributions from the several factors which influence the breadth.

At temperatures below T_m the polymer is said to exist in the ordered conformation; above T_m the disordered conformation predominates. The structural details of the temperature-induced order–disorder transition remain obscure. There is substantial evidence to suggest that the ordered form is, at least for some xanthan samples, double stranded.[13,18-25] This raises the possibility that the order-to-disorder transition may be associated with complete or partial separation of the double-stranded form. Other results have been interpreted, however, to suggest that the transition is a strictly intramolecular process.[7,10,11,26-29] Light scattering provides an obvious probe of the details of the transition, especially if strand separation is involved, since the technique yields information on the molecular weight and the molecular dimensions of the dissolved macromolecules. One also obtains the second osmotic virial coefficient, which, though more complicated to interpret, may also provide useful information about the details of the transition.

We report here a light-scattering study of xanthan covering a temperature range extending from $T_m - 34$ °C to $T_m + 25$ °C; under the conditions of these experiments $T_m \simeq 45$ °C. We have chosen to use ultrasonically degraded xanthan which has been fractionated to obtain fractions of relatively narrow molecular weight distribution (MWD). Fractions are advantageous for reasons already noted. Choice of low molecular weight samples is dictated by the desire (1) to reduce T_m as far as possible into the range of temperatures accessible to the light-scattering experiment, (2) to use samples with mean-square radii of gyration in the optimal range for their determination with visible light scattering, and (3) to ensure that the samples

* To whom correspondence should be addressed.

0024-9297/87/2220-2179$01.50/0

be free, insofar as possible, from kinetic hindrances (due, for example, to chain entanglement) to the rapid achievement of conformational equilibrium at each temperature. A concommitant disadvantage of low molecular weight samples is that the sensitivity of the observable chain dimensions to chain conformation may be less than for samples of higher molecular weight.[20-22]

Experimental Section

Polymer Sample Preparation. Powdered xanthan (Kelco Keltrol, lot 76735A) was dispersed at 6.5 g/L in water containing 0.1 M NaCl and 0.02% NaN_3 (antimicrobial agent) and stirred vigorously ("Lightnin" stirrer, Mixing Equipment Co., Rochester, NY) overnight at 25 °C. The resulting solution was sonicated for a predetermined period at 0 °C in 500-mL batches containing 2–3 mL of acetone as free radical scavenger (Heat Systems Sonicator, 375 W/20 kHz, $^1/_2$-in.-diameter probe tip). Sonicated solutions were centrifuged at 10 000 rpm (Sorvall RC2-B, GS-3 rotor) for 2 h at 25 °C. The supernatant was filtered (Millipore, 0.45 μm) and dialyzed (Travenol hollow fiber dialysis unit) against 0.01 M NaEDTA to remove multivalent cations and then exhaustively against distilled water until the dialyzate did not precipitate $AgNO_3$. The resulting solution was treated with ion-exchange resin in the Na^+ form (Fisher Rexyn 101) and dialyzed exhaustively against Millipore Milli-Q water during which the final polymer concentration was adjusted to ca. 5 g/L. This solution was fractionally precipitated with acetone in the presence of 0.5 M NaCl following the procedure for fractionation by molecular weight of Sato et al.[20] The first fraction was discarded, and the others were redissolved in distilled water, dialyzed exhaustively against Milli-Q water, and adjusted to a polymer concentration of ca. 2 g/L during the dialysis process. These were filtered through 0.45-μm Millipore filters and stored at 2 °C as salt-free stock solutions, which were colorless, showed no UV absorption in the vicinity of 254 and 280 nm, gave a negative test for the presence of protein,[30] and thus appeared to be essentially free of bacterial cell components other than xanthan. Samples were drawn from these stock solutions over a period of several months with no change in the measured properties of the polymer. The concentration of the stock solutions was determined from the residue weight following evaporation of aliquots to dryness.

Three samples, sonicated for 5, 6, and 10 h, respectively, were prepared. Each was separated into three fractions, and the middle fraction (II) was studied in each case; these are designated 5HS-II, 6HS-II, and 10HS-II. The weight percentages of polymer in each of the fractions was 26%, 5HS-I; 62%, 5HS-II; 12%, 5HS-III; 5%, 6HS-I; 90%, 6HS-II; 5%, 6HS-III; 43%, 10HS-I; 46%, 10HS-II; and 11%, 10HS-III. The experimental fraction 10HS-II thus appears to have the narrowest MWD and 6HS-II the broadest. Measurement of DS_{ace} and DS_{pyr} by using ^1H NMR spectroscopy[31] found $DS_{ace} = 1.19 \pm 0.10$ and $DS_{pyr} = 0.67 \pm 0.07$ for the purified bulk xanthan and for several of the fractions, thus confirming earlier evidence[13,20-22] that molecular weight fractionation of xanthan does not simultaneously fractionate with respect to acetyl and pyruvyl content.

Optical Activity Measurements. Measurements of specific rotation $[\alpha]_{365}$ were made as a function of temperature on the xanthan stock solutions, diluted with Milli-Q water to the desired polymer concentration and to which NaCl had been added to achieve the desired salt concentration. Measurements were made using a Perkin-Elmer 241MC spectropolarimeter with a jacketed 1.0-dm cell, the temperature of which was controlled with a circulating thermostat bath. Characteristic temperatures T_m for the chirooptically detected transition are shown for samples 5HS-II and 10HS-II as a function of the molarity, I, of added NaCl in Figure 1. For all measurements reported in Figure 1 the contribution of polymer to the total ionic strength of the system was less than $0.1I$.

Intrinsic Viscosity Measurements. Intrinsic viscosities were measured in Cannon-Ubbelohde suspended-level capillary viscometers with flow times long enough to obviate kinetic energy corrections (size 50 for $T < 60$ °C, size 25 for $T > 60$ °C).[32] In the range of shear rates encountered (<1000 s^{-1}) the intrinsic viscosity of xanthan in the molecular weight range of the present samples is expected to be shear independent, at least at $I = 0.1$ M.[33] Flow times were measured initially on solutions prepared by diluting salt-free xanthan stock solutions with Milli-Q water and adding NaCl to achieve the desired polymer and salt concentrations. These were filtered (0.45-μm Millipore) into a clean, dry viscometer. The initial solutions were subsequently diluted in the viscometer with aqueous NaCl at the same salt concentration for measurements of flow times on solutions of smaller polymer concentration. The temperature was varied and regulated to ±0.05 °C by suspension of the viscometer in a thermostat bath.

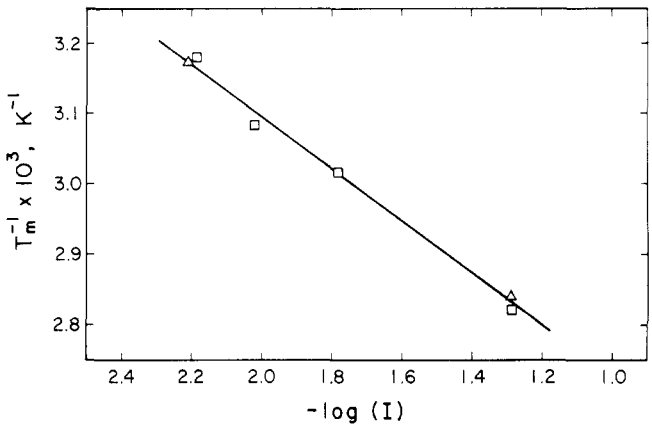

Figure 1. Plot of T_m^{-1} vs. −log (I) for 5HS-II (□) and 10HS-II (△). Line is least-squares linear fit to the data.

Light-Scattering Measurements. Light-scattering measurements were carried out using a SOFICA Model 42000 photogoniometer with unpolarized light at $\lambda = 436$ nm using floatable cells for centrifugal clarification and procedures described earlier.[13,34,35] In the present case, however, the output of the photomultiplier tube measuring the scattering intensity was read directly by a Keithley Model 480 Picoammeter and fed to a Digital MINC laboratory computer for data processing. The temperature of the scattering cell was maintained at the desired value by circulating thermostated water through the coils of the refractive index matching vat containing toluene. The temperature was always measured in the vat.

Measurements were made as a function of temperature on the xanthan stock solutions, diluted with Milli-Q water to the desired polymer concentration, to which NaCl had been added to achieve the desired salt concentration. Solutions thus prepared were filtered through 0.45-μm Millipore filters directly into the cleaned scattering cells prior to centrifugal clarification.[34]

At a given temperature the dependence of excess scattering intensity $i(\theta)$ on scattering angle θ and polymer concentration c_2 may be expressed by eq 1[36-38]

$$\frac{Kc_2}{\alpha i(\theta)} = \frac{1}{\bar{M}_w}\left(1 + \frac{\langle s^2\rangle_z}{3}\mu^2 + B\mu^4 + \ldots\right) + 2A'_2c_2 + 3Cc_2^2 + \ldots \quad (1)$$

where K and α are optical parameters defined by[34]

$$K = \frac{2\pi^2 n_B^2 i_B(90)}{N\lambda^4 R_B}\left(\frac{dn}{dc_2}\right)_\mu^2 \quad (2)$$

$$\alpha = \frac{\sin\theta}{1 + \cos^2\theta} \quad (3)$$

and μ is the magnitude of the scattering vector defined by

$$\mu = \frac{4\pi \sin(\theta/2)}{\lambda/n} \quad (4)$$

In eq 1 $\bar{M}_w$ is the weight-average molecular weight of the polymer, $\langle s^2\rangle_z$ is the z-average mean-square radius of gyration, B is a coefficient in the expansion of the Debye particle scattering factor $P(\mu)$ (given in parentheses in eq 1) in powers of μ^2, A'_2 is the light-scattering average of the osmotic second virial coefficient, and the coefficient C is related to the second and third (A'_3) osmotic virial coefficients by[38]

$$C = A'_3Q(\mu) + \tfrac{4}{3}(A'_2)^2\bar{M}_wP(\mu)[1 - P(\mu)] \quad (5)$$

where $Q(\mu)$ is a scattering factor due to interparticle interference. Other quantities appearing in eq 2–4 are the refractive index of benzene, n_B, the scattering intensity of benzene at $\theta = 90°$, $i_B(90)$, Avogadro's number, N, the wavelength of the incident light in vacuo, λ, the Rayleigh ratio for benzene, R_B, the specific refractive index increment of the polymer solution at constant chemical potential of diffusible components,[39,40] $(dn/dc_2)_\mu$, and the refractive index of the solution, n.

In the limit $c_2 = 0$ eq 1 takes the form

$$\left(\frac{Kc_2}{\alpha i(\theta)}\right)_{c_2=0} = \frac{1}{\bar{M}_w}\left(1 + \frac{\langle s^2\rangle_z}{3}\mu^2 + B\mu^4 + \ldots\right) \quad (6)$$

We have thus obtained $\langle s^2\rangle_z$ from the coefficient of the linear term in a least-squares second-degree fit to data, obtained by extrapolation at each angle to $c_2 = 0$, in the form $[Kc_2/\alpha i(\theta)]_{c_2=0}$ vs. μ^2. Since both $Q(\mu)$ and $P(\mu)$ approach unity as μ approaches zero,[36] $C = A'_3$ in this limit, where eq 1 then becomes, for data at each concentration extrapolated to $\mu = \theta = 0$,

$$\left(\frac{Kc_2}{\alpha i(\theta)}\right)_{\mu=0} = \frac{1}{\bar{M}_w} + 2A'_2c_2 + 3A'_3c_2^2 + \ldots \quad (7)$$

from which A'_2 is obtained from the coefficient of the linear term in a least-squares second-degree fit to data in the form $[Kc_2/\alpha i(\theta)]_{\mu=0}$ vs. c_2. An arithmetic mean of the constant term obtained by fitting the data evaluated according to eq 6 and 7 yielded $\bar{M}_w$.

Measurements of the Specific Refractive Index Increment. A Brice-Phoenix differential refractometer, calibrated with aqueous KCl solutions using the data of Kruis,[41] was used to measure $(dn/dc_2)_\mu$ at $\lambda = 436$ nm as a function of temperature. The desired temperature was achieved by circulating thermostated water through the refractometer cell housing, where all temperature measurements were made. Unless otherwise stipulated, solutions for refractive increment measurements were prepared by addition of NaCl to the salt-free xanthan stock solutions to achieve the desired concentration of added salt. These solutions were then brought to dialysis equilibrium in a constant-volume dialysis cell with aqueous NaCl solutions of the same concentration by using procedures described earlier.[13,35] Instrument deflections d, relative to dialyzate, were measured for the dialyzed stock solution and for dialyzed stock solution diluted quantitatively with dialyzate. These were converted to refractive index differences Δn with the calibration constant r ($\Delta n = r\Delta d$), and the refractive increment was computed from the relationship $(dn/dc_2)_\mu = \Delta n/c_2$.

Temperature Dependence of the Parameters of Eq 1–7. Application of eq 1–7 to measure $\bar{M}_w$, $\langle s^2\rangle_z$, and A'_2 as a function of temperature requires that the temperature dependence of the parameters c_2, n_B, n, $i_B(90)$, R_B, and $(dn/dc_2)_\mu$ be taken properly into account.

Xanthan stock solution concentrations were determined at room temperature (ca. 23 °C), and all dilutions of the stock solutions were carried out at the same temperature. Concentrations c_2 (g/mL) were assigned at other temperatures by assuming that the thermal expansion coefficients of the polymer solutions were identical with that of pure water.

At 25 °C the refractive index of the polymer solution, n, can be approximated with trivial error by the refractive index of aqueous NaCl at the same salt concentration, the value of which at $\lambda = 436$ nm was estimated from tabulated values at various wavelengths,[42] recognizing the λ^{-2} dependence of n.[43] To obtain n at temperatures other than 25 °C, it was assumed that the temperature coefficient of n at $\lambda = 436$ nm is the same as the known value for water at $\lambda = 589.3$ nm.[44]

Ehl et al.[45] have shown that the Brice-Phoenix calibration constant r is sensibly independent of temperature over the temperature range 25–70 °C. We have consequently determined r at 23 °C and used that value throughout the temperature range investigated here, 10–70 °C. We were unable to obtain reliable data on the temperature dependence of $(dn/dc_2)_\mu$ from experiments in which dialysis equilibrium was established at temperatures significantly different from 23 °C. It was therefore necessary to approximate $(dn/dc_2)_\mu$ at other temperatures by making measurements at a series of temperatures on solutions that had been brought to dialysis equilibrium at 23 °C. We call this quantity $(dn/dc_2)'_\mu$.

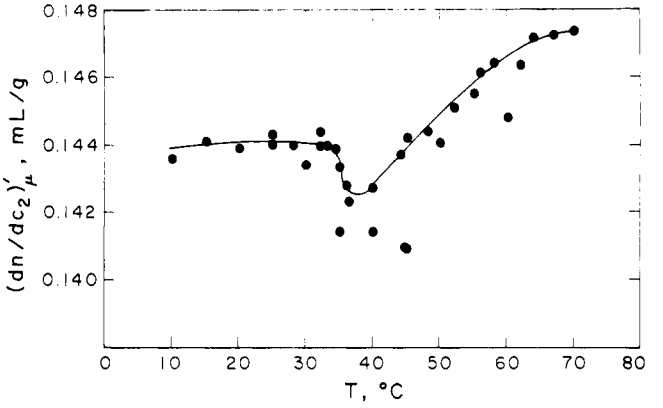

Figure 2. Plot of differential refractive index increment $(dn/dc_2)'_\mu$ vs T for 10HS-II in aqueous 0.005 M NaCl. At each T $(dn/dc_2)'_\mu$ was read from the line drawn by inspection through the data.

Results for solutions containing 0.005 M NaCl are shown in Figure 2. An increase of $(dn/dc_2)'_\mu$ from 0.144 to 0.147 mL/g is observed over the temperature range 10–70 °C. Repeated measurements suggest that the minimum near 40 °C may be real, but it is too small to have any significant effect on the measured values of $\bar{M}_w$. Earlier findings[13] that $(dn/dc_2)_\mu$ is indistinguishable from $(dn/dc_2)_c$ (measured without prior dialysis) in 0.10 M NaCl at 25 °C were confirmed in the present studies at 23 °C. This implies very little preferential interaction of xanthan with the diffusible solvent components[39,40] and suggests that the data in Figure 2 represent an excellent approximation to $(dn/dc_2)_\mu$. The very small temperature coefficient of the refractive increment was confirmed in measurements of (dn/dc_2) on the two-component system xanthan–H_2O as a function of temperature. These measurements yielded an essentially linear decline in (dn/dc_2) from 0.156 to 0.153 mL/g over the temperature range from 10 to 70 °C. Values of $(dn/dc_2)'_\mu$ from Figure 2 have been used to analyze all light-scattering data reported here, including those in systems of higher NaCl concentration, inasmuch as we find no significant dependence of $(dn/dc_2)_\mu$ on NaCl concentration between 0.005 and 0.10 M at 23 °C.

The Rayleigh ratio of benzene in eq 2 is defined by $R_B = a^2i_B(90)/I_0$, where a is the distance from the aperture of the scattered-light detector to the observed scattering volume and I_0 is the intensity of the incident radiation. Since R_B is known and $i_B(90)$ is measurable, this relation is used in the derivation of eq 1 to eliminate I_0 from the fundamental equation for the excess scattering intensity of the polymer solution; a^2 cancels in this substitution and does not appear in eq 1.[46] The refractive index of benzene, n_B, enters eq 2 through a correction for the difference between the divergence at the cell–toluene interface of light scattered from benzene in measuring $i_B(90)$ and from the polymer solution in measuring $i(\theta)$. This correction leads also to cancellation of n^2, which would otherwise appear in eq 2.[46] Ehl et al.[45] provide information on $[R_B(T)/n_B^2(T)]/[R_B(25)/n_B^2(25)]$ which, coupled with known values of $R_B(25)$[47] and $n_B(25)$,[43] permits R_B/n_B^2 to be evaluated at each temperature of interest. In practice one normally measures the scattering, $i_s(90)$, from a cylindrical glass scattering standard instead of $i_B(90)$, the ratio of these two being readily measureable at any temperature in the current range of interest. At any given temperature $i_s(90)$ was measured frequently to follow, and permit corrections for, drift in I_0 with time.

Results

Variation of $\bar{M}_w$, $\langle s^2\rangle_z^{1/2}$, and A'_2 with Salt Concentration. Measurements of $\bar{M}_w$, $\langle s^2\rangle_z$, and A'_2 were made on sample 5HS-II as a function of added salt (NaCl) concentration I at 23 and 51 °C. Salt-free xanthan stock solution, crystalline NaCl, and Milli-Q water were mixed in a volumetric flask to give solutions with the desired concentrations of xanthan and NaCl. These were immediately filtered into clean scattering cells and clarified

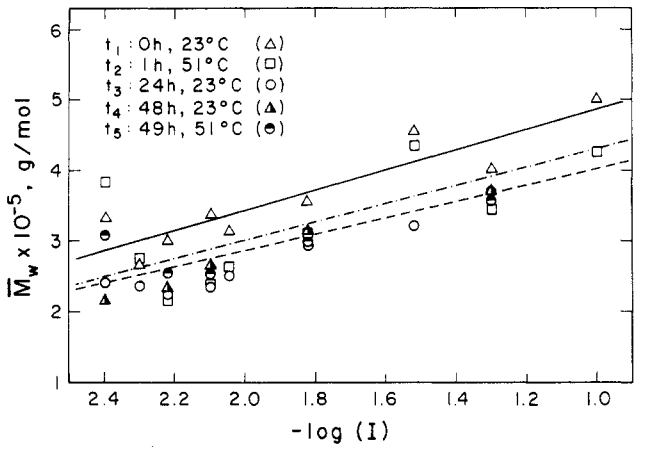

Figure 3. Plot of $\bar{M}_w$ vs. -log (I) for 5HS-II for conditions specified in the key. Least-squares linear fits to the data at t_1 (solid line), $t_2 - t_5$ (dashed line), and $t_1 - t_5$ (dash-dot line).

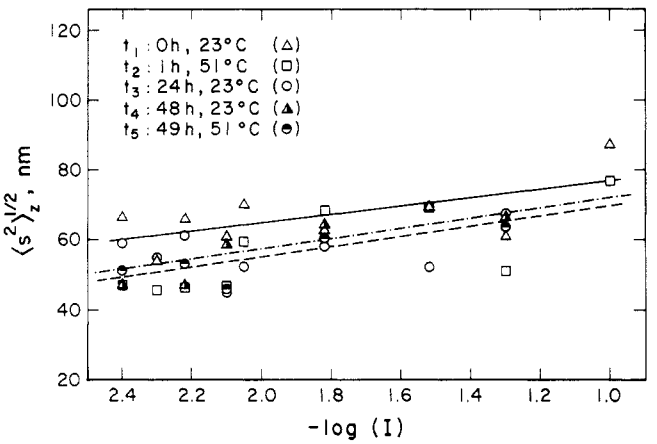

Figure 4. Plot of $\langle s^2 \rangle_z^{1/2}$ vs. -log (I) for 5HS-II for conditions specified in the key. Lines are described in legend to Figure 3.

further by centrifugation for 1.5 h, and light scattering was measured at 23 °C. The time of this initial measurement was designated t_1 (0 h). Directly following the measurement at t_1 the scattering cells were tempered in a thermostat at 51 °C and light scattering was measured at 51 °C. This measurement occurred at time t_2 (1 h). The cells from t_2 were placed in a rack on the bench top at 23 °C and allowed to remain overnight. Light scattering was measured the next day at 23 °C at a time designated t_3 (24 h). The cells from t_3 were allowed to stand another 24 h at 23 °C before measurements were again made at this temperature at time t_4 (48 h). Finally, the cells from t_4 were brought for a second time to 51 °C where light scattering was measured at time t_5 (49 h).

The results of these measurements are summarized in Figures 3, 4, and 5, where $\bar{M}_w$, $\langle s^2 \rangle_z^{1/2}$, and A'_2 are plotted, respectively, against log(I). Here the ionic strength of NaCl ranges from 0.004 to 0.1 M. Both the molecular weights (Figure 3) and the root-mean-square radii of gyration (Figure 4) show a general tendency to increase with increasing salt concentration. There is no evidence that the values of these two parameters depend upon the temperature of measurement or the elapsed time between preparation of the solutions and the measurement, *except* that both $\bar{M}_w$ and $\langle s^2 \rangle_z^{1/2}$ measured at t_1 are distinctly larger than the respective values measured subsequently. Thus, the solid curves in Figures 3 and 4 correspond to linear-least-squares regression lines through the data at t_1 while the dashed curve is the least-squares correlation of the data at $t_2 - t_5$. The scatter of the respective data points about these lines gives a clear indication of the precision we were

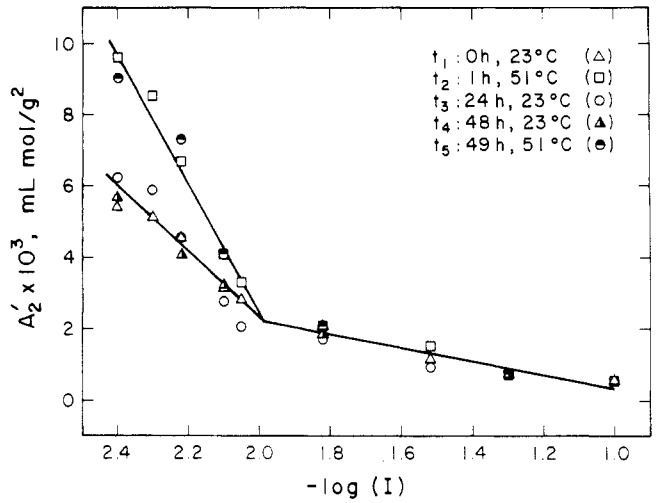

Figure 5. Plot of A'_2 vs. -log (I) for 5HS-II for conditions specified in the key. Lines drawn through data by inspection.

able to achieve in these experiments. The dash-dot line is the least-squares regression of all of the data. It is noteworthy that the dependence of $\langle s^2 \rangle_z^{1/2}$ on added salt concentration is contrary to that normally anticipated for a polyelectrolyte in aqueous solution. The observed dependence is, however, consistent with the evidence from Figure 3 for increased association of the dissolved species with increasing ionic strength.

The light scattering osmotic second virial coefficient (Figure 5) declines with increasing salt concentration as normally expected for a polyelectrolyte. For $I < 0.01$ M A'_2 is sensitive to the temperature of the measurement, but for all I the measurements at t_1 are indistinguishable from subsequent measurements (t_3, t_4) at the same temperature. Sensitivity of A'_2 to T below $I = 0.01$ M is undoubtedly related to the dependence of T_m on I (Figure 1).[6,7,10,11] Thus, for all $I > 0.01$ M, 51 °C is below T_m, and at this temperature the system remains predominantly in the ordered state. As I falls below 0.01M, an increasing proportion of xanthan is converted to the disordered state at 51 °C.

Variation of $\bar{M}_w$, $\langle s^2 \rangle_z^{1/2}$, and A'_2 with Temperature. In order to bring T_m into the middle of the readily accessible temperature range for light scattering (10–70 °C) it is necessary to work at rather low ionic strength. On the basis of Figures 3–5 it is evident that among the light-scattering observables A'_2, at least, is sensitive to T in the accessible temperature range for $I = 0.005$ M. This salt concentration is, however, still large enough to ensure a manageable combination of virial coefficients and polymer concentrations. Thus, at $I = 0.005$ M it was possible to make reliable light-scattering measurements by using polymer concentrations of (1–6) $\times 10^{-4}$ g/mL. These were large enough to produce excess scattering with satisfactory signal-to-noise ratio and small enough so that the contribution of the polymer to the total ionic strength of the system never exceeded one-fifth that due to the added NaCl. Choice of a lower I would have necessitated still lower polymer concentrations, both in order to satisfy the latter condition and to obtain reliable measurements of the initial slope and intercept of the concentration dependence (eq 7), with concomitant reduction in experimental precision.

Figures 6–8 show $\bar{M}_w$, $\langle s^2 \rangle_z^{1/2}$, and A'_2 for sample 6HS-II as a function of T at $I = 0.005$ M; specific rotation $[\alpha]_{365}$ for the same sample is shown as a function of T on each plot. Solutions were prepared and clarified by centrifugation at room temperature as described in the previous

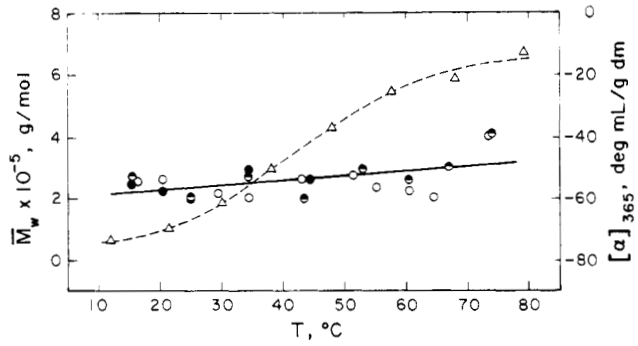

Figure 6. Plot of $\bar{M}_w$ vs. T for 6HS-II in 0.005 M NaCl corresponding to first (○), second (◓), and third (●) heating. Line is least-squares linear fit to all of the data. Corresponding plot of $[\alpha]_{365}$ vs. T (△) also shown with curve drawn by inspection.

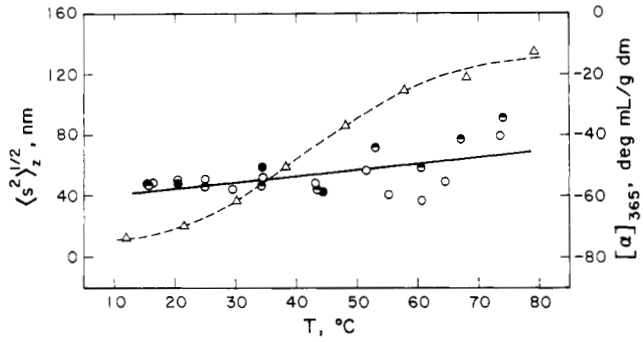

Figure 7. Plot of $\langle s^2 \rangle_z^{1/2}$ vs. T for 6HS-II in 0.005 M NaCl corresponding to first (○), second (◓), and third (●) heating. Line is least-squares linear fit to all of the data. Corresponding plot of $[\alpha]_{365}$ vs. T (△) as in Figure 6.

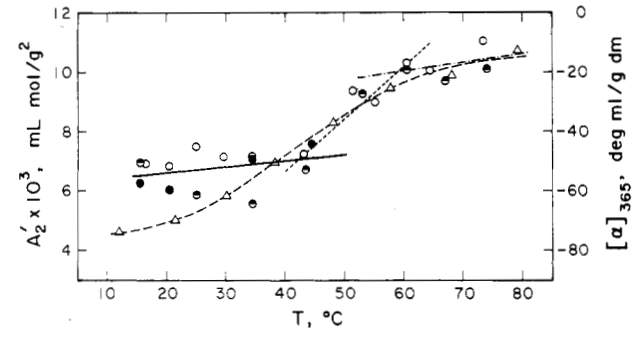

Figure 8. Plot of A'_2 vs. T for 6HS-II in 0.005 M NaCl corresponding to first (○), second (◓), and third (●) heating. Linear least-squares fits to data below 44 °C (solid line), between 44 and 62 °C (short dashed line), and above 62 °C (dash–dot line). Corresponding plot of $[\alpha]_{365}$ vs. T (△) as in Figure 6.

section. Light-scattering measurements were made immediately at some temperature and again the same day at one or two other temperatures, each higher than the temperature of the previous measurement. Each such series of measurements was made without allowing the sample to cool between the measurements. The results of such measurements are designated "first heating" in Figures 6–8. Following measurements made during the first heating, the cells were placed in a rack on the bench top at ambient conditions. The next day measurements were made on the same solutions at a second series of ascending temperatures and these are designated "second heating". After standing again over night at 23 °C the cells were frequently subjected to measurements in a "third heating" series. The optical activity results in Figures 6–8 are data gathered exclusively in the first heating.

Once a given set of solutions was prepared, filtered, sealed in the cells, and centrifuged, all measurements in

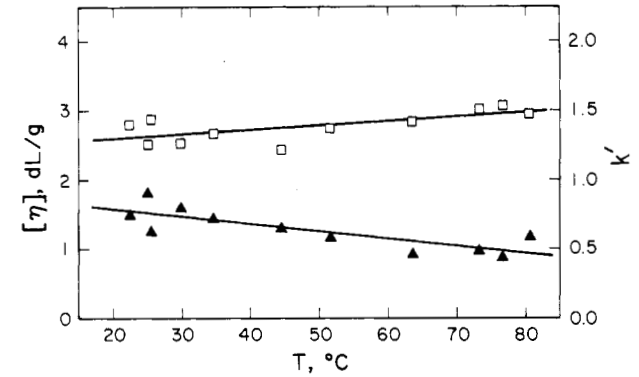

Figure 9. Plots of $[\eta]$ (□) and Huggins constant k′ (▲) vs. T for 6HS-II in 0.005 M NaCl. Lines are linear least squares fits to the data.

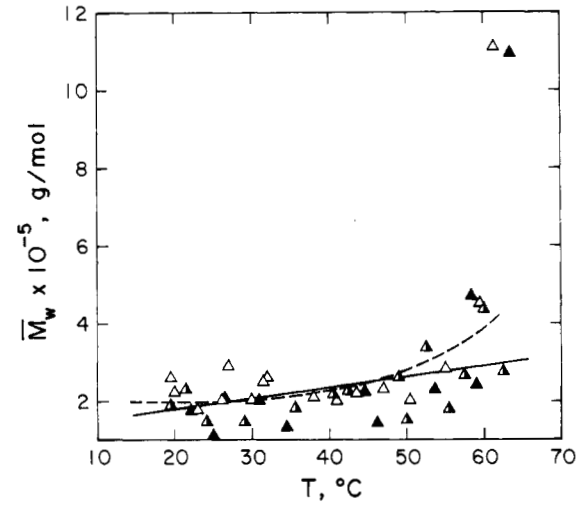

Figure 10. Plot of $\bar{M}_w$ vs. T for 10HS-II in 0.005 M NaCl corresponding to first (△), second (▲), and third (▲) heating. Solid line is linear least squares fit to all of the data except the two largest values of $\bar{M}_w$; dashed curve drawn by inspection.

the first, second, and third heating series were done without further clarification. The reproducibility of these measurements may be deduced from the scatter of points about the linear-least-squares regression lines through the data in Figures 6–8. In the case of Figure 8 different least-squares lines are drawn in three different temperature ranges to emphasize the evidence for a "transition" in A'_2, the low-temperature onset of which about 44 °C is near the midpoint, T_m, of the chirooptically detected transition. Neither $\bar{M}_w$ (Figure 6) nor $\langle s^2 \rangle_z^{1/2}$ (Figure 7) displays a transition, as anticipated from Figures 3 and 4. Each, nevertheless, shows a small tendency to increase with increasing T, although the positive slopes of the regression lines in Figures 6 and 7 are largely a consequence of the two points at the highest temperatures. The temperature dependence of the intrinsic viscosity, shown in Figure 9, clearly mimics that of $\bar{M}_w$ and $\langle s^2 \rangle_z^{1/2}$ and provides some confirmation that the trend in $\langle s^2 \rangle_z^{1/2}$ is real. In contrast to the data in Figures 3 and 4, there is no evidence here that the initial low-temperature measurements on a given sample yield higher $\bar{M}_w$ and $\langle s^2 \rangle_z^{1/2}$ than do subsequent measurements at low temperature following heating.

Sample 6HS-II has a relatively broad MWD, which is expected to soften the features of any temperature-driven conformational transition that may occur. Similar measurements of the temperature dependence of the light-scattering parameters of 10HS-II are therefore reported in Figures 10–12. Duplicate osmotic pressure measurements[13] at 30 °C in 0.005 M NaCl yield, in conjunction with

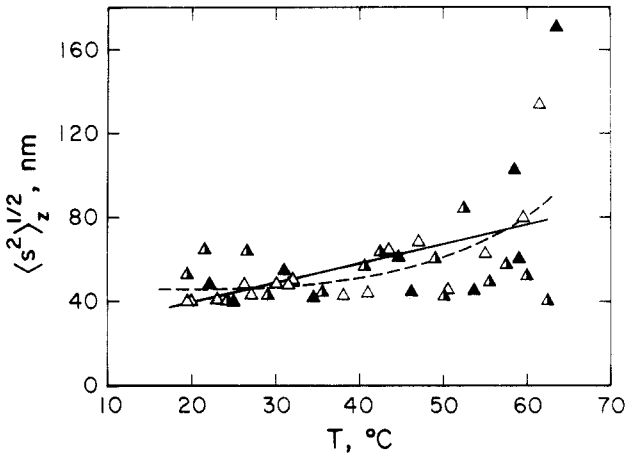

Figure 11. Plot of $\langle s^2 \rangle_z^{1/2}$ vs. T for 10HS-II in 0.005 M NaCl corresponding to first (△), second (▲), and third (▲) heating. Solid line is linear least-squares fit to all of the data; dashed curve drawn by inspection.

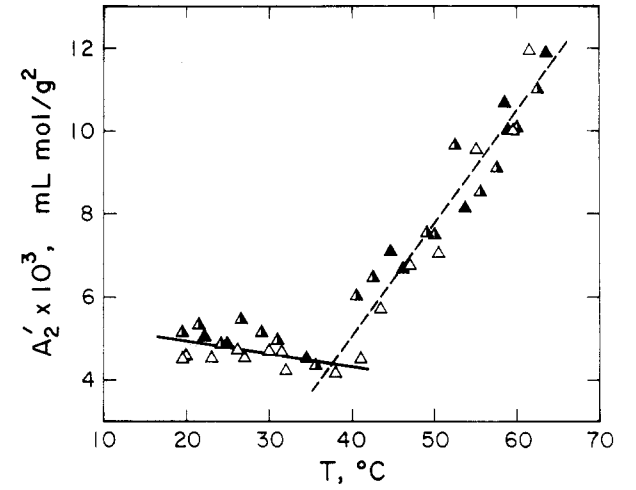

Figure 12. Plot of A'_2 vs. T for 10HS-II in 0.005 M NaCl corresponding to first (△), second (▲), and third (▲) heating. Linear least-squares fits to data below 40 °C (solid line) and above 40 °C (dashed line).

extensive light-scattering data under these conditions, $\bar{M}_w/\bar{M}_n = 1.20 \pm 0.05$ for 10HS-II. The trends observed for 6HS-II are repeated with 10HS-II, but a more pronounced increase in both $\bar{M}_w$ and $\langle s^2 \rangle_z^{1/2}$ occurs near the upper end of the experimental temperature range. The transition in A'_2 evident with 6HS-II is significantly better defined for 10HS-II, although the high-temperature plateau region is not observed, presumably because the highest temperatures investigated were only about 62 °C. Again, the low-temperature onset of the transition in A'_2 is close to T_m as defined by the transition detected chirooptically. Plots of $[\alpha]_{365}$ vs. T are shown for 10HS-II in Figure 13, where it is clearly seen that the excursion in $[\alpha]_{365}$ is greater for the first heating than for the subsequent heatings. Also noteworthy is the reproducibility of the optical activity data for heatings two and three. (Second and third heating $[\alpha]_{365}$ data for 6HS-II, not shown in Figures 6–8, resemble those for 10HS-II in Figure 13.) It likewise appears from Figure 10 that the initial experiments at low T yield slightly higher values of $\bar{M}_w$ than subsequent measurements at low temperatures; this effect is not apparent for $\langle s^2 \rangle_z^{1/2}$ in Figure 11. These data for 10HS-II are all at least consistent with the anomalous character of the $\bar{M}_w$ and $\langle s^2 \rangle_z^{1/2}$ data for 5HS-II at t_1 in Figures 3 and 4. That is, after the first heating one does not return to the original state of the system through incubation of the sample at 23 °C for a period of at least 24 h, but subsequent heating cycles are quite reproducible.

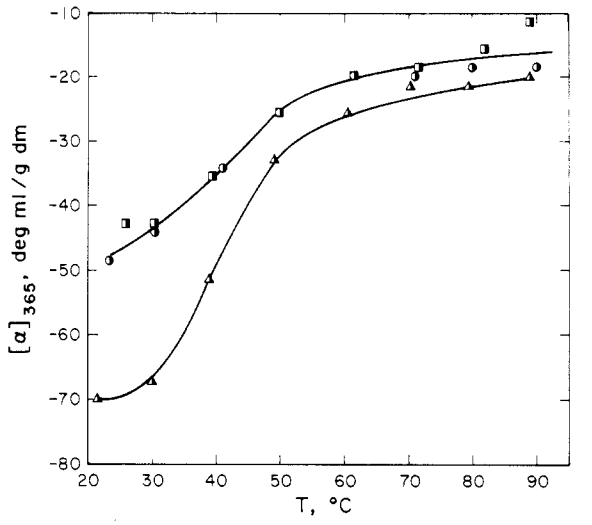

Figure 13. Plot of $[\alpha]_{365}$ vs. T for 10HS-II in 0.005 M NaCl corresponding to first (△), second (◨), and third (◑) heating with curves through data drawn by inspection.

Discussion

The data presented in Figures 6–13 do not display the decline in $\bar{M}_w$ with T that might be expected on passing through T_m, if the chirooptically observed transition were associated with the disruption of a double-stranded ordered form. Indeed, there is evidence, albeit rather weak, that both $\bar{M}_w$ and $\langle s^2 \rangle_z^{1/2}$ increase with increasing T, especially at temperatures above T_m. Only the virial coefficient A'_2 shows any evidence of a "transition" in the sense of that postulated from the T dependence of $[\alpha]_{365}$, but the midpoint temperature T'_m of the transition in A'_2 is approximately 10 deg greater than the chirooptically detected T_m at the same concentration of added NaCl (I = 0.005 M). Figures 3–5 disclose that both $\bar{M}_w$ and $\langle s^2 \rangle_z^{1/2}$ increase with an increase in the salt concentration in the range 0.004 M $\leq I \leq$ 0.100 M, whereas A'_2 shows the sharp decline anticipated for a polyelectrolyte. Within the observed range of temperature and salt concentration $\bar{M}_w$ and $\langle s^2 \rangle_z^{1/2}$ at a given T and I proved to be sensibly independent of the thermal history of the sample, provided the sample had once been heated to T_m or beyond; there was no indication of any dependence of A'_2 at a given T and I on thermal history.

Evidence for the double-stranded character of the ordered form of xanthan samples prepared by sonication is now very strong;[13,18–25] recent electron microscope visualizations of single- and double-stranded xanthan chains are especially persuasive.[24,25] We consequently believe that it is necessary to provide an interpretation of the present results in the context of a model that incorporates a double-stranded ordered form. It is quite evidently possible to accommodate the present results to the viewpoint that the chirooptically detected transition is an intramolecular process in which the chain is single stranded in both the ordered and disordered states,[7,10,11,26–29] so we will omit a discussion of the all-single-strand model. Despite the evidence presented above for incomplete reversibility of the initial temperature-driven transition as followed by $[\alpha]_{365}$, $\bar{M}_w$, and $\langle s^2 \rangle_z^{1/2}$, the full reversibility of subsequent passages through T_m encourages us to seek an equilibrium model.

We offer here a model which assumes that segments from two xanthan chains can associate to form ordered duplex structures, the existence of which in solution is

strongly suggested by investigations using light scattering,[13,20-23] hydrodynamics,[19,20,21] and electron microscopy[18,24,25] and in the solid state by X-ray fiber diffraction studies.[48] The model is capable of explaining, at least qualitatively, all of our temperature-dependence data, including the putative increase in $\bar{M}_w$ at or above T_m and the strong temperature dependence of A'_2. Precedents for the approach taken can be found elsewhere in the literature of the biopolymers. In particular, Shibata and Schurr[49] demonstrate that a variety of interesting experimental phenomena observed near the denaturation temperatures of DNA and collagen can be attributed to aggregation of the multistranded native polymers, which is favored by the configurational degeneracy of the system at and above the transition temperature. We adopt a somewhat more general approach and extend the statistical mechanical treatment of Applequist and Damle[50] to allow for the existence of aggregates or clusters containing an arbitrary number of single-stranded chains of arbitrary chain length. Details of the mathematical treatment and a discussion of its quantitative applicability to the present data will be presented elsewhere.[51]

We observe initially that we do not necessarily identify changes in $[\alpha]_{365}$ with changes in the extent of double-strand character in the system. It is clear that some 65% of the mass of xanthan occurs in the side chains, which, in contrast to the conformationally extended and quite rigid cellulosic backbone, have considerable inherent conformational freedom.[52] Thus, changes in $[\alpha]_{365}$ are likely to arise predominantly from changes in side-chain conformation, and we assume that these may occur in both single- and double-stranded segments of the molecule to produce changes in $[\alpha]_{365}$ that may not be proportional to changes in the amount of double-stranded structure.

If we assume that each xanthan repeating unit has the capacity to associate with one and only one repeating unit from another xanthan chain, then it is possible to identify double-stranded xanthan chain sequences, in which one or more adjacent repeating units are engaged in these intermolecular associations, and single-stranded sequences, in which no such associations are present. Clusters involving any number of xanthan chains may form under these circumstances, subject to the requirement that the points of intermolecular association are invariably double-stranded sequences and constrained as to the average number of chains participating in a cluster only by the single-strand concentration and chain length distribution, the inherent strength of the association constant s for pairing of xanthan repeat units, and the magnitude of a parameter $\beta < 1$, which measures the loss of entropy in the system for each double-stranded sequence formed by a pair of xanthan chains.[50] To simplify the model we assume that any pair of xanthan chains can form between themselves only one double-stranded sequence of arbitrary length and that no single chain can form a double-stranded sequence with itself; the inherent approximation should be small for the relatively short and stiff xanthan chains comprising the present experimental samples, which have on the average only about 200 backbone glucose residues per single-stranded chain.

It is readily shown, provided the enthalpy change $\Delta H_s°$ for association of xanthan residues is always negative, that the low-temperature equilibrium state of this system, even if heterogeneous with respect to single-strand chain length, will consist predominantly of double-stranded dimers comprising two chains of identical chain length and possessing the maximum number of associations. At high enough temperatures the system must, of course, dissociate completely to single strands. At intermediate temperatures, e.g., near the point where half the maximum possible number of residue–residue associations exists, equilibrium is characterized, even at moderate polymer concentration, by the existence of many clusters containing more than two chains and for which $\bar{M}_w$, and presumably $\langle s^2\rangle_z^{1/2}$, can exceed substantially the values characterizing the "homogeneous dimers" predominating at low-temperature equilibrium. For simplicity the model assumes that $\Delta H_s°$ and β are independent of T, although this restriction can be lifted at the cost of additional parameters in the theory, and this dictates the form of the predicted T dependence of cluster size distribution. The dependence of mean cluster size on ionic strength, pH, and other environmental factors is not explicitly treated here, but s is presumably an implicit function of these variables.

It is not our current purpose to offer a quantitative application of the model to the present experimental data. We observe, however, that the present results are qualitatively consistent with the model: Both $\bar{M}_w$ and $\langle s^2\rangle_z^{1/2}$ appear to increase for $T > T'_m$, although we obviously have not demonstrated the existence of the necessary maximum in $\bar{M}_w$ (and, depending on single-strand extension and flexibility, in $\langle s^2\rangle_z^{1/2}$) vs. T, presumably because use of toluene as the index-matching liquid precluded studies at temperatures above about 70 °C. (Failure to dissociate the double strands completely may also be due to a more complicated temperature dependence of s than incorporated into the model.) If one assumes, consistent with earlier evidence,[13,19-22] that the present xanthan samples have chain lengths small enough to exhibit rodlike behavior in their low-temperature ordered form, then one can calculate the mass per unit length M_L from the experimental observables and the relationship[13]

$$M_L = \left(\frac{\bar{M}_z\bar{M}_{z+1}}{12\langle s^2\rangle_z}\right)^{1/2} \tag{8}$$

Assuming a log-normal MWD for which $\bar{M}_w/\bar{M}_n = \bar{M}_z/\bar{M}_w = \bar{M}_{z+1}/\bar{M}_z$,[53] we compute for 10HS-II, using the low-temperature data from Figures 10 and 11, $M_L \simeq 1850$ nm^{-1}; a slightly larger value is obtained if the Zimm–Schulz MWD is assumed. This result is fully consistent with the M_L expected for rodlike double-stranded xanthan[13,19-25] and is thus in accord with the low-temperature behavior of the present model.

The temperature dependence of A'_2 can also be explained qualitatively, if we assume that the Donnan contribution[54] to the virial coefficient is dominant in the present system at 0.005 M NaCl. Using the Devore–Manning theory[55] of the nonideal Donnan contribution to A'_2 ($A'_{2,D}$) in conjunction with reasonable estimates[9] of the Manning charge density parameter ξ[56] for single- ($\xi \simeq 1.1$) and double-stranded ($\xi \simeq 2.4$) xanthan, we calculate, respectively, $A'_{2,D} = 79.3 \times 10^{-3}$ and 16.7×10^{-3} mL mol/g^2. These results depend only on the salt concentration (here $I = 0.005$ M) and on xanthan structural features, which determine ξ and the equivalent weight; they are independent of xanthan molecular weight. For double strands the greater proportion of "condensed" counterions[55,56] reduces the effective polymeric (nondiffusible) charge and, hence, the Donnan effect. With the full theory of the order-to-disorder transition,[51] which allows one to calculate the proportions of single and double strands in the system, one then concludes that $A'_{2,D}$ should display a sigmoidal temperature dependence, the sharpness of which depends on c_2, MWD, β, and $\Delta H_s°$. The ratio of the limiting high- and low-temperature plateau values of $A'_{2,D}$ is given by $A'_{2,D}$ (single)/$A'_{2,D}$ (double) = 4.75, in reasonable agreement

with the experimental observations for 10HS-II. The sigmoidal temperature dependence of $A'_{2,D}$ can be used to define the characteristic midpoint temperature T'_m, which corresponds to formation of one-half the maximum possible number of interstrand associations (i.e., "bonds") and which is not necessarily identical with T_m from chirooptical measurements.

As invariably found,[54,55] the calculated $A'_{2,D}$ is several times larger than the measured A'_2; in the present case $A'_{2,D}/A'_2 \simeq 3$–7. In some cases this disagreement may arise in part from the alternating character of the virial expansion for the Donnan contribution to the osmotic pressure, Π_D, and the slow convergence of this series.[55] Thus, plots of Π_D/c_2 vs. c_2 calculated from this expansion for single- and double-stranded xanthan[57] are both effectively linear over a wide range of c_2. Linear fits to these plots interpreted to yield $A_{2,D}$ underestimate the true $A_{2,D}$ by a factor of about 2. This exercise makes clear the difficulty of extracting the second virial coefficient in polyelectrolyte systems at low salt concentration where the Donnan contribution is large.[55] We have confirmed with these calculations that all of the data reported here were gathered in a range of c_2 where the dependence of Π_D/c_2 on c_2 is dominated by the linear term in the Devore–Manning expansion.

Besides the Donnan contribution to A'_2, already discussed, one must of course be concerned with a negative contribution expected to arise from the postulated equilibrium cluster formation.[58] Our calculations[51] show that, for the temperature and concentration ranges encountered in the experiments reported here, this negative contribution is a factor of 10 or more smaller in magnitude than $A'_{2,D}$. Estimates of the polyion–polyion contribution to A'_2 using the theory of Odijk and Houwaart[59] show this contribution likewise to be much smaller than $A'_{2,D}$. Thus, our assumption that $A'_{2,D}$ dominates A'_2 appears to be justified. The equilibrium cluster model may also suggest that light-scattering data, ostensibly extrapolated to infinite dilution of the macromolecule, should yield $\bar{M}_w$ for the putative single strand regardless of the temperature. This expectation overlooks the high probability for interstrand bonds even well beyond the conformational transition temperature due to the large configurational degeneracy of the system.[49] An average of less than one-half interstrand bond per chain is required to yield a light-scattering molecular weight corresponding to the dimeric cluster; it may well be necessary to dilute the sample beyond the range of tolerable signal-to-noise ratio to achieve an accurate extrapolation into the concentration range where single strands predominate.

We conclude with a comment on the irreproducibility of measurements of $\bar{M}_w$ and $\langle s^2\rangle_z^{1/2}$ at t_1 in the experiments reported in Figures 3 and 4 and of the $[\alpha]_{365}$ vs. T data for the first heating in Figure 13. In contrast to this is the striking reproducibility of all of the A'_2 data. It appears that before our samples were first heated to ca. 50 °C, they were slightly more aggregated, as measured by $\bar{M}_w$ and $\langle s^2\rangle_z^{1/2}$ at t_1, and more "ordered", as measured by $[\alpha]_{365}$ in the first heating, than they were after having been heated. We do not know whether to attribute this aggregation to some irreversible aspect of the same mechanism postulated in our above model or to some quite different aggregation process. If the present model proves accurate, then one must conclude from the reproducibility of the virial coefficient data that the postulated single-to-double stranded chain association process is fully reversible for low molecular weight xanthan samples, and this allows one to allocate the initial aggregation before heating to a different mechanism. In any case, this initial aggregation is no hindrance to equilibrium solution measurements on low molecular weight xanthan, inasmuch as it is readily dispersed on mild heating and does not return over a period of several days when the samples are incubated at room temperature. We are at present inclined to believe that the salt dependence of $\bar{M}_w$ and $\langle s^2\rangle_z^{1/2}$, revealed in Figures 3 and 4, reflects primarily the effect of an aggregation process different from the one postulated in the model advanced here.

Acknowledgment. This work has been supported by NIH Grant GM33062. Fellowship support from the NIH–French CNRS Program for Scientific Collaboration is gratefully acknowledged by D.A.B., who thanks the members of the staff of the CERMAV (Grenoble) for their hospitality during preparation of parts of this paper. Support for G.E.W. by the NSF Predoctoral Fellowship program is also acknowledged with thanks.

Registry No. Xanthan gum, 11138-66-2.

References and Notes

(1) Sandford, P. A., Laskin, A. I., Eds. *Extracellular Microbial Polysaccharides*; American Chemical Society: Washington, DC, 1977; ACS Symp. Ser., No. 45.
(2) Brant, D. A., Ed. *Solution Properties of Polysaccharides*; American Chemical Society: Washington, DC, 1981; ACS Symp. Ser., No. 150.
(3) Jansson, P. E.; Kenne, L.; Lindberg, B. *Carbohydr. Res.* **1975**, *45*, 275.
(4) Melton, L. D.; Mindt, L.; Rees, D. A., Sanderson, G. R. *Carbohydr. Res.* **1976**, *46*, 245.
(5) Jeanes, A.; Pittsley, J. E.; Senti, F. R. *J. Appl. Polym. Sci.* **1961**, *5*, 519.
(6) Holzwarth, G. *Biochemistry* **1976**, *15*, 4333.
(7) Morris, E. R.; Rees, D. A.; Young, G.; Walkinshaw, M. D.; Darke, A. *J. Mol. Biol.* **1977**, *110*, 1.
(8) Southwick, J. G.; McDonnell, M. E.; Jamieson, A. M.; Blackwell, J. *Macromolecules* **1979**, *12*, 305.
(9) Paoletti, S.; Cesaro, A.; Delben, F. *Carbohydr. Res.* **1983**, *123*, 173.
(10) Norton, I. T.; Goodall, D. M.; Frangou, S. A.; Morris, E. R.; Rees, D. A. *J. Mol. Biol.* **1984**, *175*, 371.
(11) Milas, M.; Rinaudo, M. *Carbohydr. Res.* **1986**, *158*, 191.
(12) Milas, M.; Rinaudo, M. In ref 2, Chapter 3.
(13) Paradossi, G.; Brant, D. A. *Macromolecules* **1982**, *15*, 874.
(14) Dentini, M.; Crescenzi, V.; Blasi, D. *Int. J. Biol. Macromol.* **1984**, *6*, 93.
(15) Sandford, P. A.; Pittsley, J. E.; Knutson, C. A.; Watson, P. R.; Cadmus, M. C.; Jeanes, A. In ref 1, Chapter 15.
(16) Holzwarth, G.; Ogletree, J. *Carbohydr. Res.* **1979**, *76*, 277.
(17) Gravanis, G.; Milas, M.; Rinaudo, M.; Tinland, B. *Carbohydr. Res.* **1987**, *160*, 259.
(18) Holzwarth, G.; Prestridge, E. B. *Science (Washington, D.C.)* **1977**, *197*, 757.
(19) Holzwarth, G. *Carbohydr. Res.* **1978**, *66*, 173.
(20) Sato, T.; Norisuye, T.; Fujita, H. *Polym. J.* **1984**, *16*, 423.
(21) Sato, T.; Norisuye, T.; Fujita, H. *Macromolecules* **1984**, *17*, 2696.
(22) Liu, W.; Sato, T.; Norisuye, T.; Fujita, H. *Carbohydr. Res.* **1987**, *160*, 267.
(23) Coviello, T.; Kajiwara, K.; Burchard, W.; Dentini, M.; Crescenzi, V. *Macromolecules* **1986**, *19*, 2826.
(24) Stokke, B. T.; Elgsaeter, A.; Smidsrød, O. *Int. J. Biol. Macromol.* **1986**, *8*, 217.
(25) Stokke, B. T.; Elgsaeter, A.; Skjåk-Braek, G.; Smidsrød, O. *Carbohydr. Res.* **1987**, *160*, 13.
(26) Milas, M.; Rinaudo, M. *Carbohydr. Res.* **1979**, *76*, 189.
(27) Rees, D. A. *Pure Appl. Chem.* **1981**, *53*, 1.
(28) Norton, I. T.; Goodall, D. M.; Morris, E. R.; Rees, D. A. *J. Chem. Soc., Chem. Commun.* **1980**, 545.
(29) Milas, M.; Rinaudo, M. *Polym. Bull.* **1984**, *12*, 507.
(30) Bradford, M. M. *Anal. Biochem.* **1976**, *72*, 248.
(31) Rinaudo, M.; Milas, M.; Lambert, F.; Vincendon, M. *Macromolecules* **1983**, *16*, 816.
(32) Cannon, M. R.; Manning, R. E.; Bell, J. D. *Anal. Chem.* **1960**, *32*, 355.
(33) Milas, M.; Rinaudo, M.; Tinland, B. *Polym. Bull.* **1985**, *14*, 157.
(34) Goebel, K. D.; Brant, D. A. *Macromolecules* **1970**, *3*, 634.
(35) Jordan, R. C.; Brant, D. A. *Macromolecules* **1980**, *13*, 491.

(36) Zimm, B. H. *J. Chem. Phys.* **1948**, *16*, 1093.
(37) Evans, J. M. In *Light Scattering from Polymer Solutions*; Huglin, M. B., Ed.; Academic: New York, 1972; Chapter 5.
(38) Siano, D. B.; Applequist, J. *Macromolecules* **1975**, *8*, 858.
(39) Casassa, E. F.; Eisenberg, H. *Adv. Protein Chem.* **1964**, *19*, 287.
(40) Strazielle, C. In *Light Scattering from Polymer Solutions*; Huglin, M. B., Ed.; Academic: New York, 1972; Chapter 15.
(41) Kruis, A. *Z. Phys. Chem.* **1936**, *34B*, 13.
(42) Meyer, R. J., Ed. *Gmelins Handbuch der Anorganischen Chemie, Natrium*; Verlag Chemie GMBH: Berlin, 1928; Vol. 21, p 349.
(43) Johnson, B. L.; Smith, J. In *Light Scattering from Polymer Solutions*; Huglin, M. B., Ed.; Academic: New York, 1972; Chapter 2.
(44) Weast, R. C., Ed. *CRC Handbook of Chemistry and Physics*, 58th ed.; CRC Press: Cleveland, OH, 1977; p E-223.
(45) Ehl, J.; Loucheux, C.; Reiss, C.; Benoit, H. *Makromol. Chem.* **1964**, *75*, 35.
(46) Eisenberg, H.; Felsenfield, G. *J. Mol. Biol.* **1967**, *30*, 17.
(47) Utiyama, H. In *Light Scattering from Polymer Solutions*; Huglin, M. B., Ed.; Academic: New York, 1972; Chapter 4.
(48) Okuyama, K.; Arnott, S.; Moorhouse, R.; Walkinshaw, M. D.; Atkins, E. D. T.; Wolf-Ullish, Ch. In *Fiber Diffraction Methods*; French, A. D., Gardner, K. N., Eds.; American Chemical Society: Washington, DC, 1980; Chapter 26, ACS Symp. Ser., No. 141.
(49) Shibata, J. H.; Schurr, J. M. *Biopolymers* **1981**, *20*, 525.
(50) Applequist, J.; Damle, V. *J. Am. Chem. Soc.* **1965**, *82*, 1450.
(51) Washington, G. E.; Brant, D. A., manuscript in preparation.
(52) Pérez, S.; Vergelati, C. *Int. J. Biol. Macromol.*, in press.
(53) Elias, H.-G.; Bareiss, R.; Watterson, J. G. *Adv. Polym. Sci.* **1973**, *11*, 111.
(54) Tanford, C. *Physical Chemistry of Macromolecules*; Wiley: New York, 1961; Chapter 4.
(55) Devore, D. I.; Manning, G. S. *Biophys. Chem.* **1974**, *2*, 42.
(56) Manning, G. S. *Q. Rev. Biophys.* **1978**, *11*, 179.
(57) Hacche, L. S. Ph.D. Dissertation, University of California, Irvine, 1986.
(58) Elias, H.-G. In *Light Scattering from Polymer Solutions*; Huglin, M. B., Ed.; Academic: New York, 1972; Chapter 9.
(59) Odijk, T.; Houwaart, A. C. *J. Polym. Sci., Polym. Phys. Ed.* **1978**, *16*, 627.

Use of Multidetector Light-Scattering Experiments To Study the Flexibility of Individual Polymer Chains in Solution

William G. Griffin,* Mary C. A. Griffin,† and François Boué‡

EMRI, Brunel University, Egham, Surrey TW20 0JZ, UK, AFRC Institute of Food Research, Reading Laboratory, Shinfield, 0HE, RG2 9AT, UK, and TCM Group, Cavendish Laboratory, Cambridge CB3 0HE, UK. *Received December 24, 1986*

ABSTRACT: A general expression for the four-particle electric field amplitude correlation function for light scattered by Gaussian polymer chains is given and used to evaluate the intensity cross-correlation function measured in a two-detector dynamic light-scattering experiment for flexible (Rouse) and semiflexible (Harris–Hearst) polymer chains. The results are compared with those for a rigid-rod scatterer, and the possibility of using two-detector, cross-correlation techniques to distinguish between rigid, semiflexible, and flexible polymers is discussed. A procedure for approximating the four-particle function for a Gaussian chain is given with a numerical example of the time-dependent contribution of the first mode of a Rouse chain to the decay of the intensity correlations. For the Rouse chain the time dependence of the cross-correlation function exhibits a $(kR_g)^2$ dependence on the scattering vector for $\mathbf{k}_1 \cong \mathbf{k}_2$ and $kR_g \gtrsim 4$.

Introduction

Conventional, single-detector, dynamic light-scattering techniques can be used to measure internal relaxations of flexible polymers in solution. Examples of such experiments are studies of DNA[1] and F actin.[2] The correlation of intensity fluctuations is measured, and, for large numbers of scatterers in the scattering volume, this intensity correlation is related to the electric field correlations by the Siegert relation.[3] Theories of polymer dynamics can be used to calculate the time dependence of the field correlation function, $g^{(1)}(\mathbf{k},t) \propto \langle E^*(\mathbf{k},0)E(\mathbf{k},t)\rangle$; for example, $g^{(1)}$ was calculated for the Rouse model by Pecora[4] and for a semiflexible chain model by Maeda and Fujime.[5] Those authors also calculated the Fourier Transform of $g^{(1)}$, which is related to the spectral distribution of the scattered light. In the present work we report results for field and intensity correlations which can be directly measured by digital correlation techniques. The electric field correlation function, $g^{(1)}(\mathbf{k},t)$, is strongly affected by the translational diffusive motion of the polymer molecules. For polarized light scattering, length and time scales of internal modes are in principle measurable for $kR_g > 1$, provided the contribution of the translational motion to $g^{(1)}(\mathbf{k},t)$ can be accurately allowed for. Such investigations offer technical problems[5,6,7] as the center-of-mass motion of the macromolecule must be accurately characterized independently of any intramolecular effects. Only then can the contribution of the center-of-mass diffusion to the time dependence of the intensity correlation function be eliminated to obtain the intramolecular time-dependent contribution. It is therefore of value to devise quasi-elastic light-scattering experiments in which the contribution of the center-of-mass motion to the observed correlations is eliminated or reduced.

The particular type of dynamic light-scattering experiment to be discussed in this paper involves the use of two (or more) photomultipliers set up to receive the light scattered by individual macromolecules passing through the same small scattering volume; the photomultiplier outputs are cross correlated (see Figure 1). The feasibility of such experiments was established by Griffin and Pusey,[8] who predicted and observed an anticorrelation in the intensity cross-correlation function, $g^{(2)}(\mathbf{k}_1,\mathbf{k}_2;t)$, $(\mathbf{k}_1\cdot\mathbf{k}_2 = 0)$, for light scattered by rotating rodlike scatterers. The theoretical results given here apply over the experimentally accessible range of both scattering vectors: thus they apply

*To whom all correspondence should be addressed at Brunel University.
†AFRC Institute of Food Research.
‡TCM Group. Present address: Centre d'Etudes Nucléaires de Saclay, Gif-Sur-Yvette, France.

0024-9297/87/2220-2187$01.50/0